SUPPORTING INFORMATION

New Models of Tetrahymena Telomerase RNA from Experimentally Derived Constraints and Modeling

Daud I. Cole†¥, Jason D. Legassie‡¥, Laura N. Bonifacio‡¥, Vijay G. Sekaran‡, Feng Ding†, Nikolay V. Dokholyan†* and Michael B. Jarstfer‡*

†Department of Biochemistry and Biophysics, School of Medicine, and ‡Division of Chemical Biology and Medicinal Chemistry, Eshelman School of Pharmacy. University of North Carolina at Chapel Hill, Chapel Hill, North Carolina

Contents

SUPPLEMENTAL METHODS

Native gel electrophoresis of telomerase complex. 2 μL of soluble, affinity purified telomerase, 1xHit Buffer, 40 U of RNasin (Promega), and 10 mM NMIA or DMSO and were incubated at 30 °C. NMIA or DMSO was added to the reactions after preincubation at 30 °C for 2 min. At increasing time points, 50% glycerol containing xylene cyanol to a final glycerol concentration of 5% and the entire reaction was immediately loaded onto a 10 cm by 10 cm native acrylamide gel (5% acrylamide/bisacrylamide (29:1), 45 mM Tris base pH 8.3, 45 mM boric acid, 1 mM EDTA, and 4% glycerol) and resolved at 150 V. For each experiment, control samples contained untreated telomerase, telomerase treated with 4.5 μg of ribonuclease A, and telomerase added to hit reactions after NMIA or DMSO was quenched for 90 minutes (5 half lives). Gels were dried under vacuum and exposed to phosphorimager plates to detect ^{35}S-Met labeled tTERT and/or ^{32}P-5'-labeled tTER-3'-Ext.

Data analysis. SHAPE intensities from SAFA quantified denaturing gels were scaled with a previously described model free box plot analysis.[1] Alternatively, we applied a 2-8% rule more appropriate for data sets smaller than 300 nucleotides where we discard the top 2% of the most reactive peaks and divide by the average intensity of the next 8%.[2-4] SHAPE intensities from free in solution TER and TER in the presence of TERT were treated separately. The arithmetic mean of SHAPE intensities at each nucleotide position was calculated from data normalized with the box plot analysis and 2-8% rule. The sample variance s^2 for each nucleotide position was calculated using equation 2. Variances above 0.01 served as markers of nucleotide positions with highly variant SHAPE reactivities across testing dates.

$$s^2 = \frac{\sum_{i=1}^{i=n}(x_i - \bar{x})^2}{n-1} \qquad (1)$$

The standard deviation (SD) of normalized SHAPE reactivities for each nucleotide position was calculated using equation 3. Intensities from highly variant nucleotides were excluded from a final arithmetic mean calculation of all nucleotide positions if they were more than three standard deviations (SD) from the previously calculated mean.

$$SD = \sqrt{\frac{\sum_{i=1}^{i=n}(x_i - \bar{x})^2}{n}} \qquad (2)$$

The arithmetic mean at each nucleotide position of free in solution SHAPE intensities was calculated from both the box plot and 2-8% values for 3 measurements of nucleotides 10-88. The means were calculated from 5 measurements of nucleotides 75-159 for each nucleotide position

Predicted secondary structure models of tTER. Base pairing probabilities for base pairs in folded tTER were predicted with the *partition* program from RNAstructure 5.3 and the output was saved as binary files.[5-7] We specified that the calculation take place at a temperature of 303 K. The SHAPE reactivities were incorporated in predictions as pseudo energy constraints using equation 4 for each base paired residue i.[8] The slope parameter m was varied from zero to five and the intercept parameter b was varied from 0 to -3 with no effect on predictions. We focused on the minimum free energy structure although a small number of similar structures were obtained because even if more accurate structures are predicted at higher folding free energies, there is no general way to identify these as improved structures. TER base pair models predicted by SHAPE and RNAstructure were compared to models developed by comparative sequence analysis, 15, 16 RNA structural probing experiments5, 6, 16, 20 before submission to DMD and were composed using the xrna software (http://rna.ucsc.edu/rnacenter/xrna/).

$$\Delta G_{SHAPE} = m * ln[SHAPE\ Reactivity(i) + 1] + b \qquad (4)$$

Base pairing probabilities were maximized to predict the most accurate structure expected using the *MaxExpect* program.[9] The program *ProbKnott* was used in an attempt to predict pseudoknots.[10] *Scorer* was used to calculate the sensitivity and positive predictive value (PPV) quality metrics when comparing predictions to accepted structures.[6,11] Flexible pairings are allowed meaning base pairs are considered to be correctly predicted when one of the two indices is different by up to one nucleotide. This better accounts for RNA dynamics and uncertainty in the RNA structure. For a known base pair a-b, all of the following predicted pairs are considered correct with flexible pairings:

a → b
a → b – 1
a → b + 1
a – 1 → b
a + 1 → b

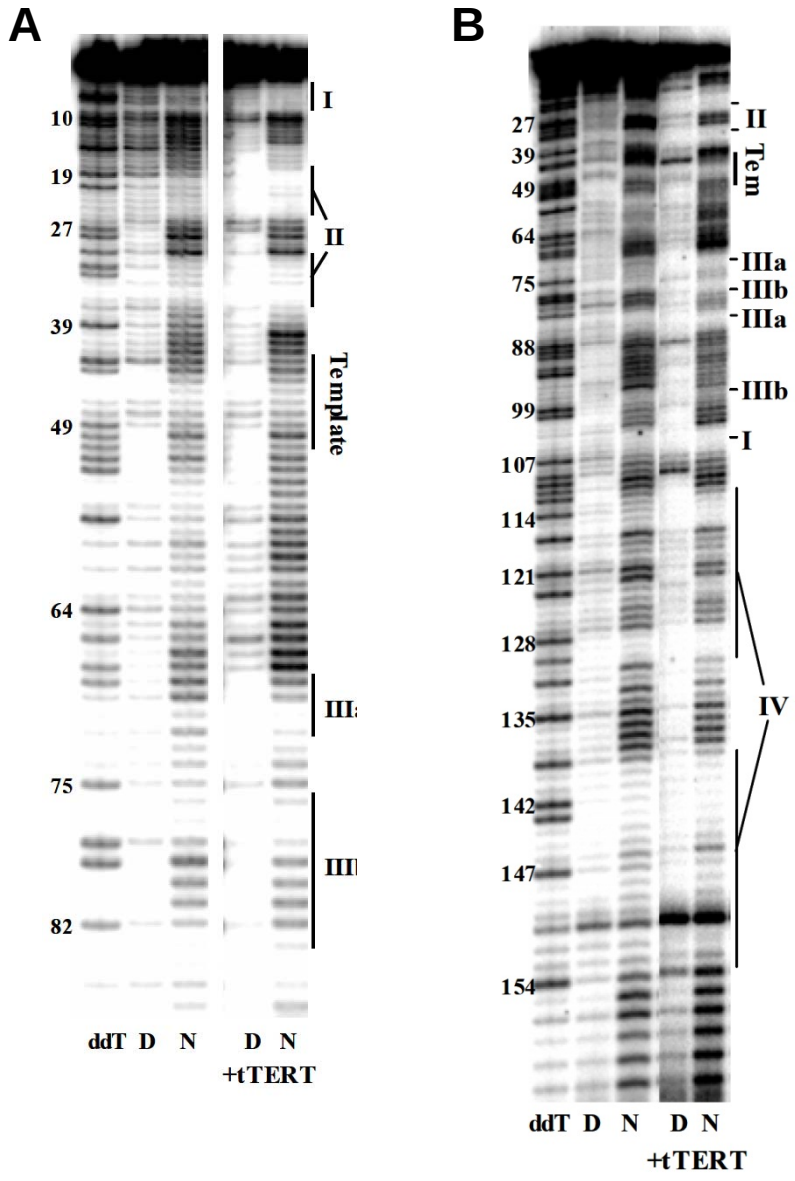

Figure S1: SHAPE reactivity of protein free and tTERT-bound tTER. (A) Sequencing gel of tTER using primer C103. (B) Sequencing gel of tTER using primer conRT. Dideoxythymidine ladder (ddT) are shown for orientation. Ladders are labeled to include a one-nucleotide shift for ease of interpretation. Each RNA was reacted with ether NMIA (N) or the carrier DMSO (D) as labeled below each lane.

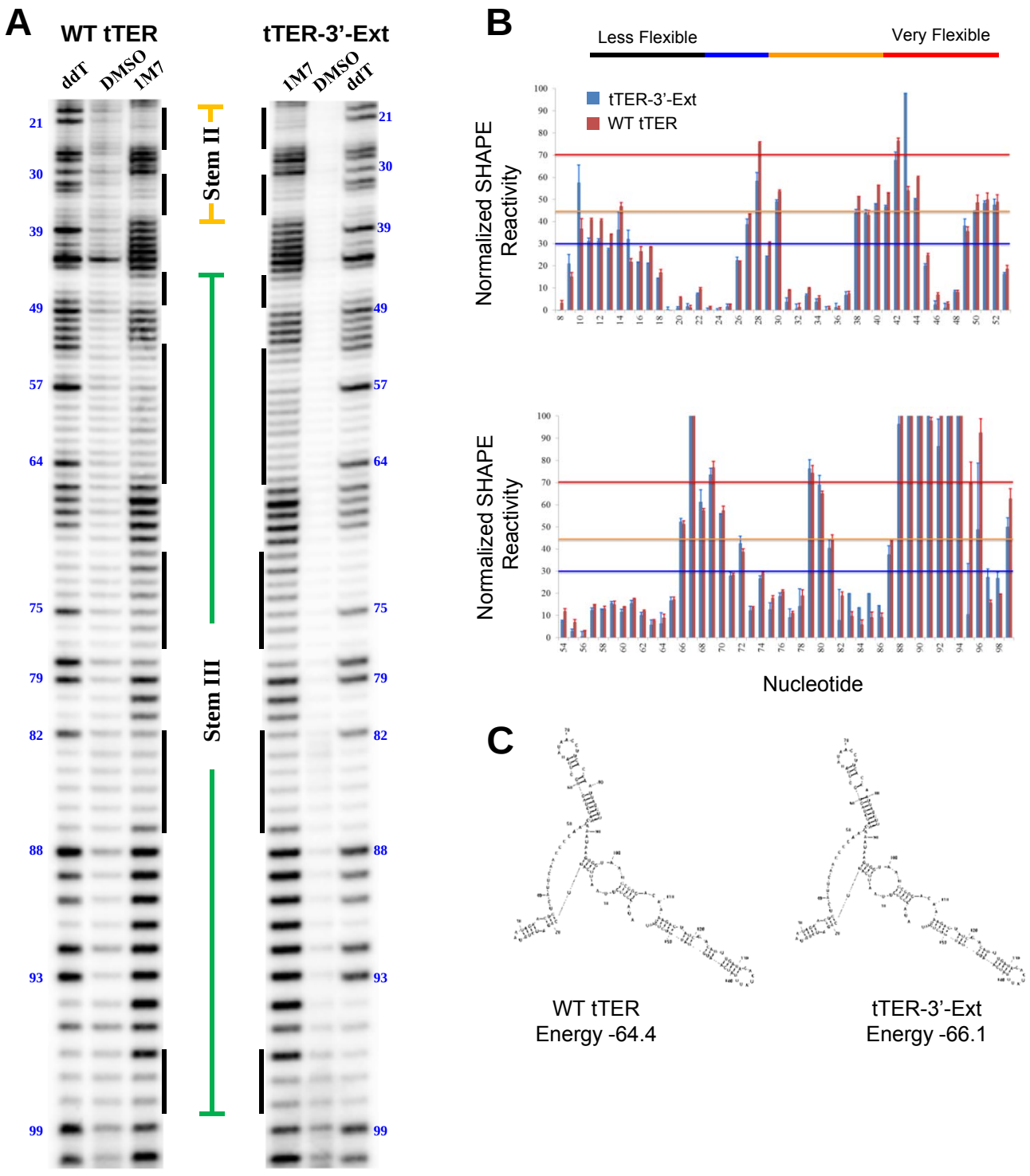

Figure S2. Comparison of the SHAPE reactivity of protein free wild-type with tTER-3'-Ext. (A) Sequencing gel of 1M7-treated tTER using primer C103. Ladders are labeled to include a one-nucleotide shift for ease of interpretation. Each RNA was reacted with either 1-methyl-7-nitroisatoic anhydride (1M7) or the carrier DMSO (DMSO) as labeled above each lane. (B) Quantified data from gels in (A). (C) RNAstructure predicted secondary structure of tTER using SHAPE constraints. Note that the 3'-Ext RNA is shown without the 3'-extension.

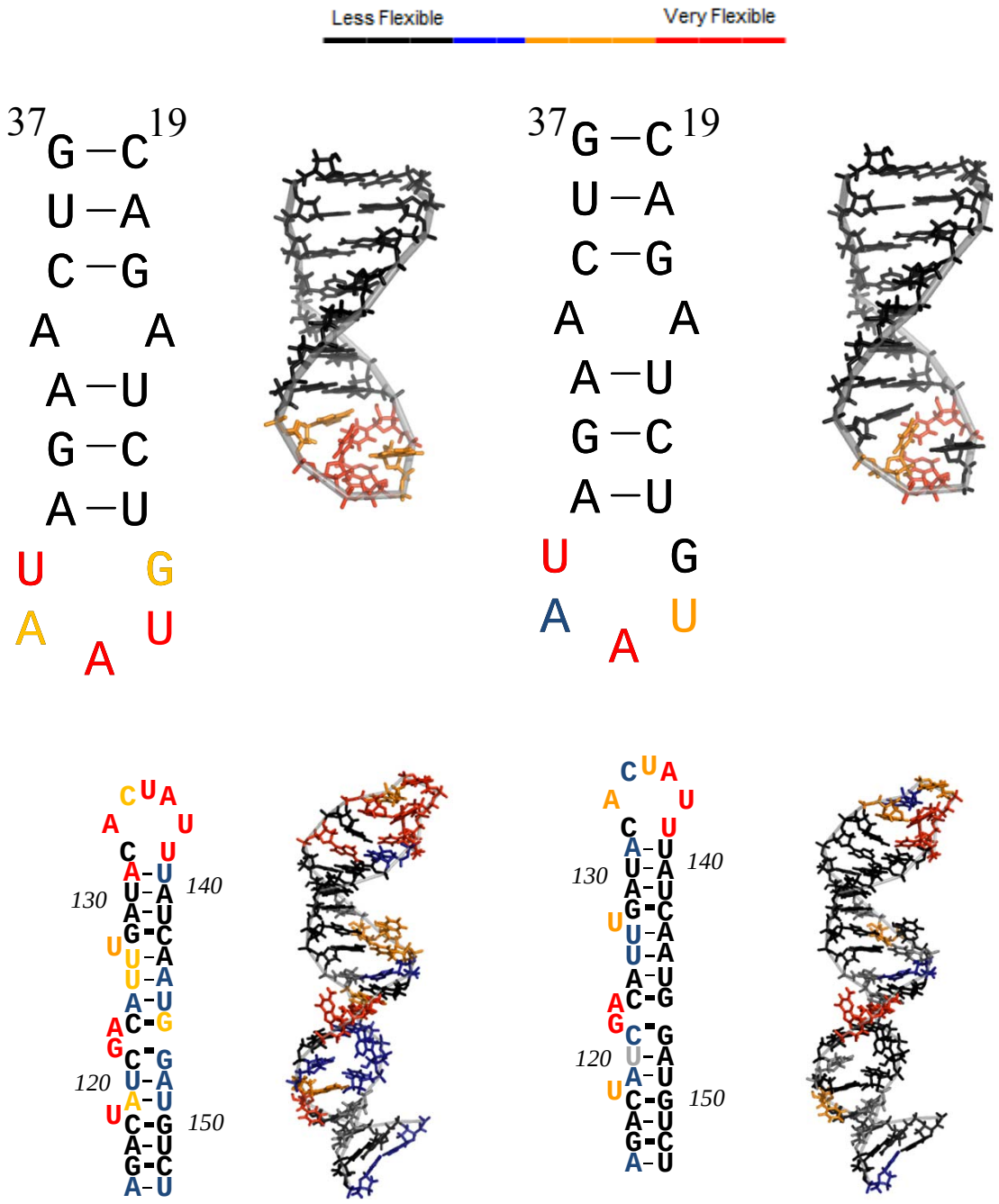

Figure S3. Comparison of SHAPE reactivity data to solution structures of tTER stems II and IV. (A) Nucleotides in the solution structure of stem II were color coded to reflect the SHAPE reactivities in the absence or presence of tTERT. (B) Nucleotides in the solution structure of stem IV were color coded to reflect the SHAPE reactivities in the absence or presence of tTERT. Structures were rendered in Pymol from PDB 2FRL and PDB 2FEY.

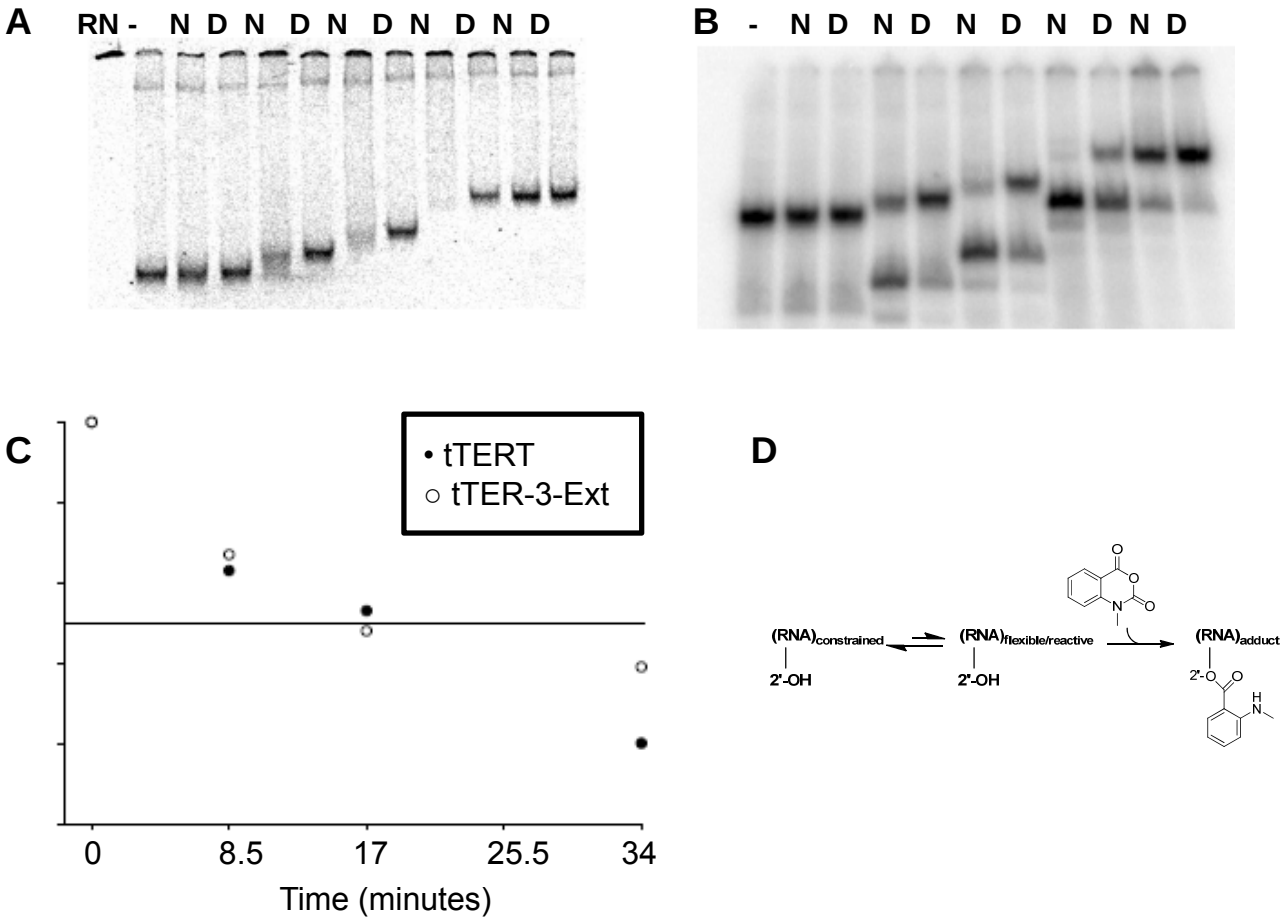

Figure S4. NMIA destabilizes the minimal telomerase complex**.** Immunopurified telomerase complex containing were treated with NMIA for various time points and the complexes were analyzed by native gel electrophoreses. (A) Fate of treated complexes using ^{35}S-tTERT to follow the reaction. tTERT enters the gel when bound to tTER, but is to acidic to enter the gel after dissociation. (B) Fate of treated complexes using ^{32}P-tTER to follow the reaction. tTER migrates in two populations: bound and unbound to tTERT. (C). Quantification of data from (A) and (B). (D). Schematic of SHAPE chemistry showing reaction of N-methyl isatoic anhydride with RNA 2'-OH.

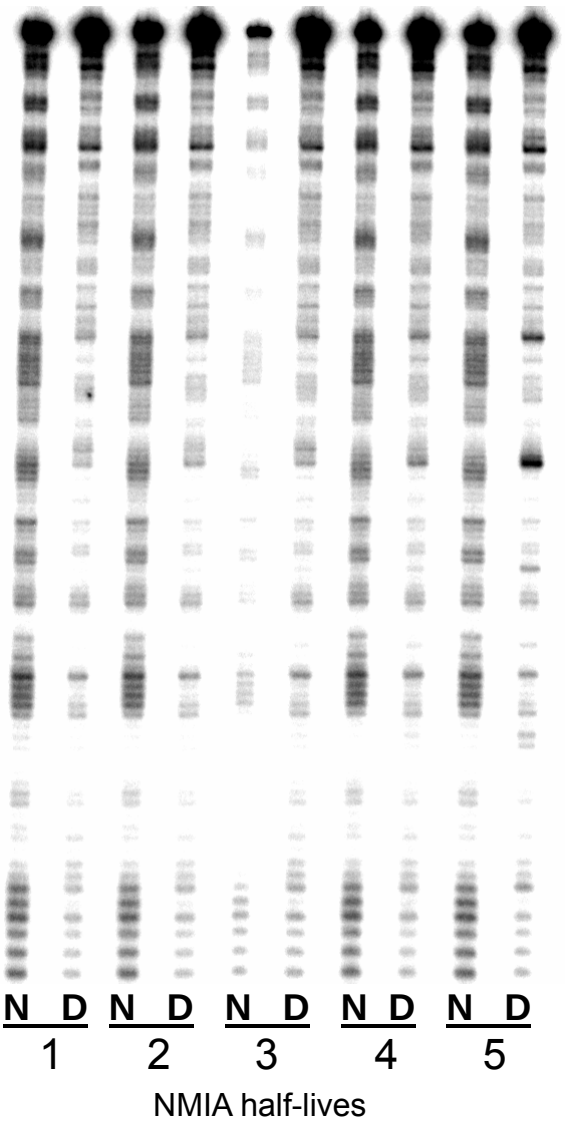

Figure S5. SHAPE footprint of tTER bound to tTERT does not change over several NMIA half-lives. Immunopurified tTERT-tTER complexes were treated with NMIA and quenched at various time points, shown as half-lives of NMIA. One half-life is ~17 min. SHAPE reactivity was determined as described in methods.

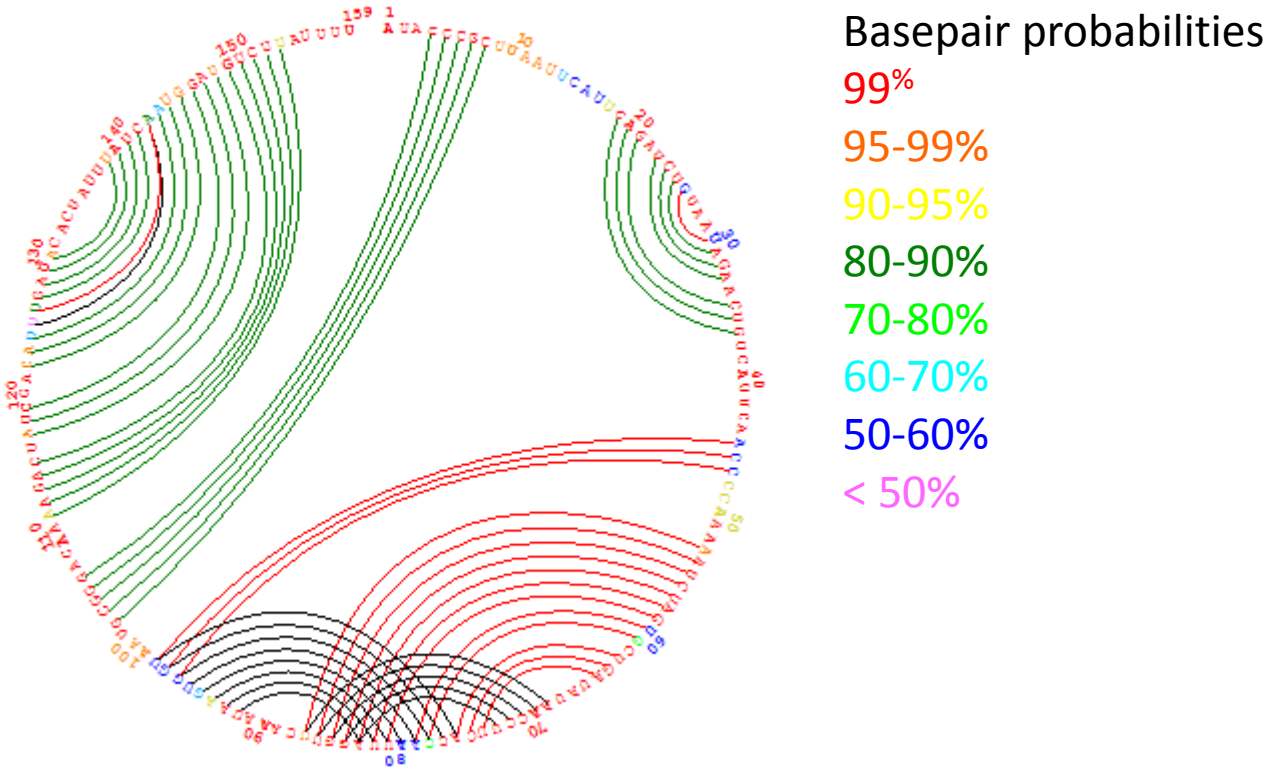

Figure S6. Circle plot of base pairs predicted for the protein-free tTER. RNAstructure was constrained by SHAPE data from protein free tTER to generate base-pairing probabilities. These are compared to base-pair assignment from comparative sequence analysis. Base pairs indicated by green lines are predicted by RNAstructure and by comparative sequence analysis. Red lines indicated base pairs present only in the SHAPE constrained RNAstructure model. Black lines indicate base pairs present only in the structure predicted from comparative sequence analysis. Nucleotides are colored (see legend) to indicate the RNAstructure determined probability of nucleotide conformation (i.e. base paired or not).

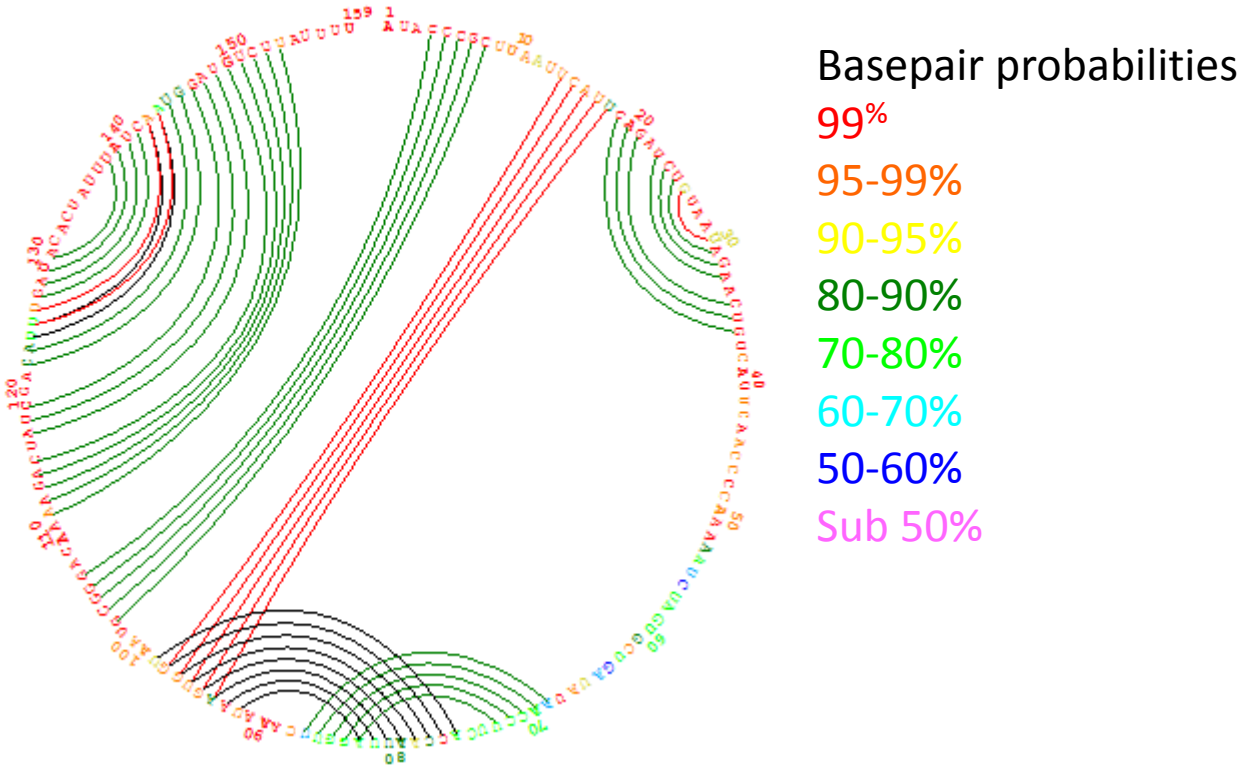

Figure S7. Circle plot of base pairs predicted for the tTER bound to tTERT. RNAstructure was constrained by SHAPE data from tTERT-bound tTER to generate base-pairing probabilities. These are compared to base-pair assignment from comparative sequence analysis. Base pairs indicated by green lines are predicted by RNAstructure and by comparative sequence analysis. Red lines indicated base pairs present only in the SHAPE constrained RNAstructure model. Black lines indicate base pairs present only in the structure predicted from comparative sequence analysis. Nucleotides are colored (see legend) to indicate the RNAstructure determined probability of nucleotide conformation (i.e. base paired or not).

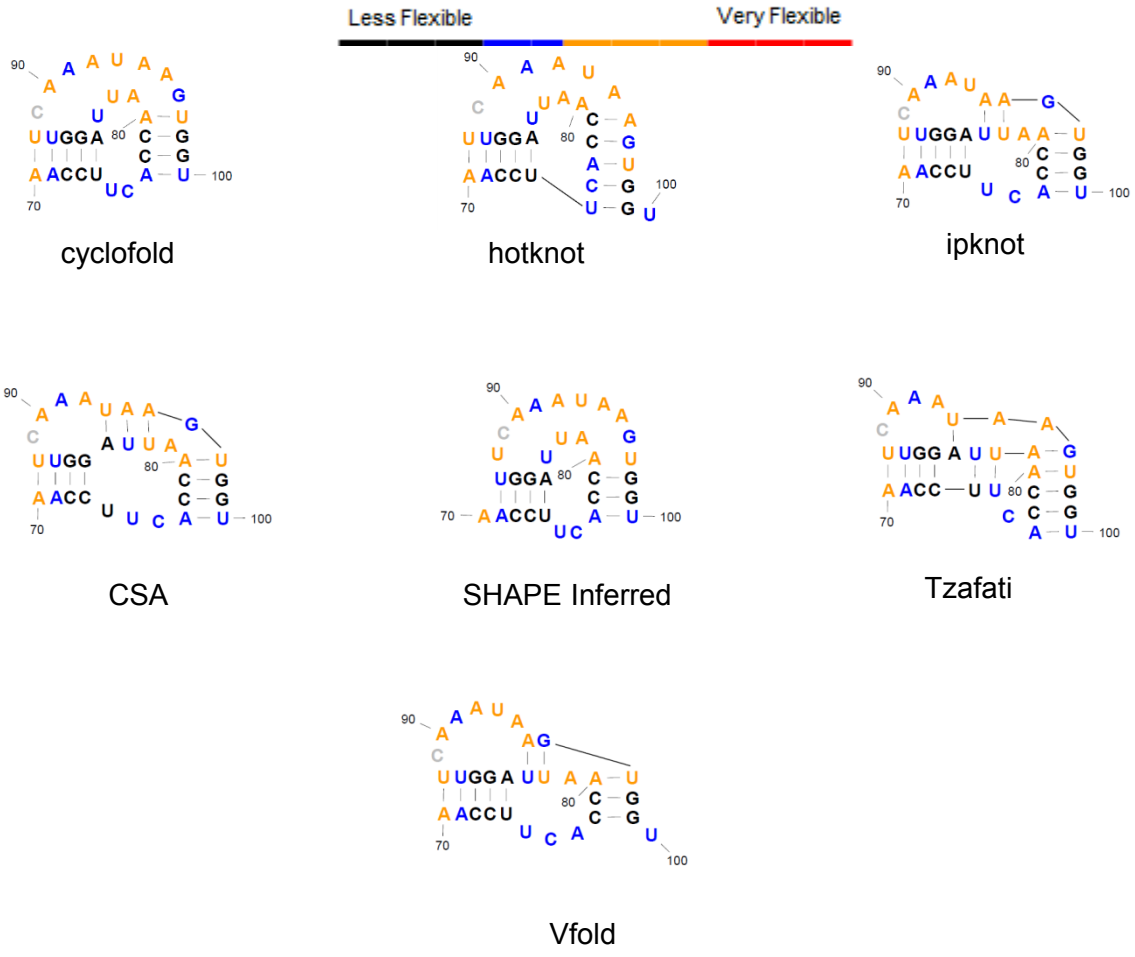

Figure S8. SHAPE reactivity is not consistent with individual models of the tTER pseudoknot. SHAPE reactivities for pseudoknot nucleotides in tTERT-bound tTER are superimposed on the indicated models for the tTER pseudoknot.

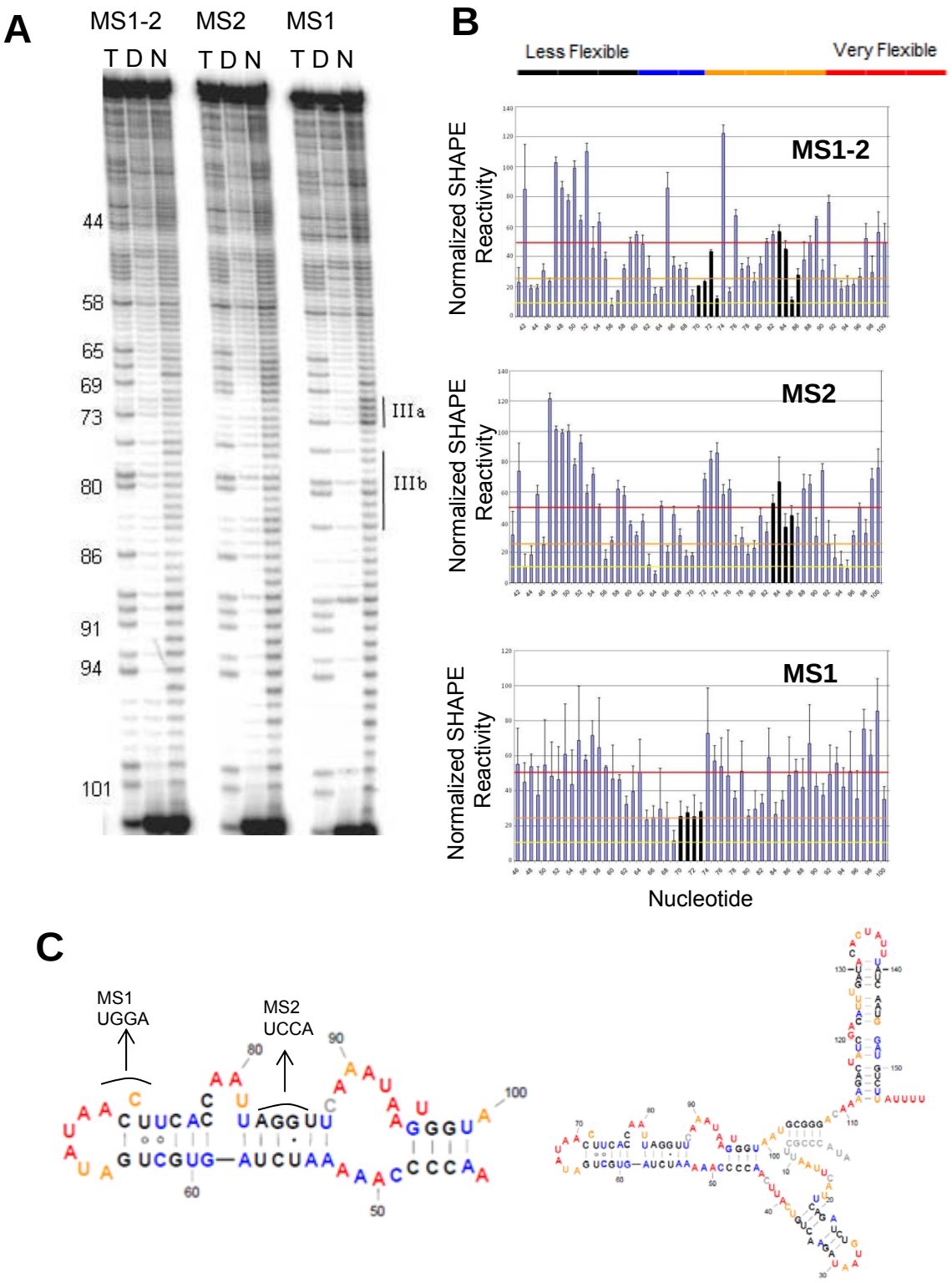

Figure S9. Analysis of tTER mutants designed to block specific base-pairs in stem III of the protein free tTER structure. (A) Sequencing gels of indicated protein-free tTER mutants using conRT as the primer. (B) Quantified data from gels in (A). (C) Description of MS1 and MS2 mutants and the secondary structure of protein free tTER. RNAs are color coded for SHAPE reactivity of the wild-type sequence.

A

Label	Nucleotides	FRET value	Calculated distance
sIII-sIV	U139 – U92	0.70 → 0.95	31 → 52 Å
TRE-sIV	U139 – U63	0.70 → 0.95	31 → 52 Å
TRE-TBE	U63 – U36	0.20 → 0.60	47 → 76 Å
tTER+p65+tTERT	U139 – U10	0.45 → 0.75	42 → 54 Å

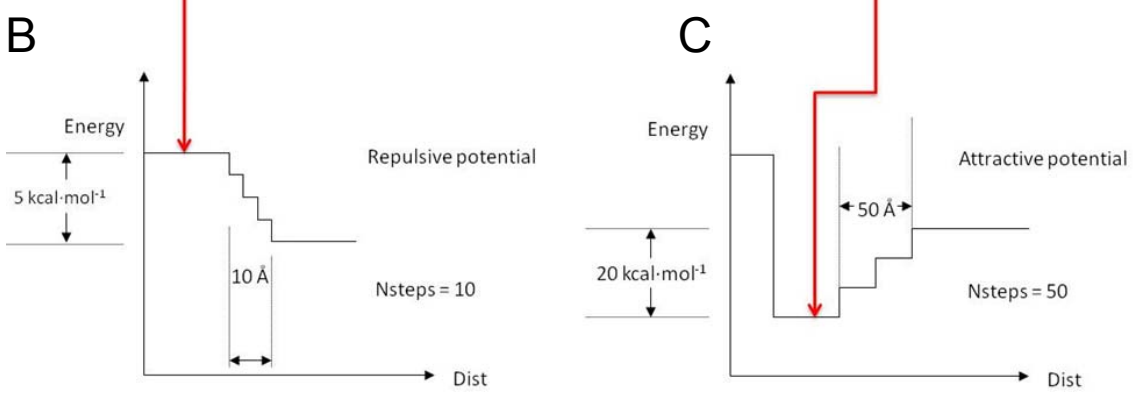

Figure S10. FRET potential functions used as constraints for DMD experiments. (A) Calculated distances between FRET fluorophores. (B) Energy diagram for the repulsive interaction potential. (C) Energy diagram for the attractive interaction potential.

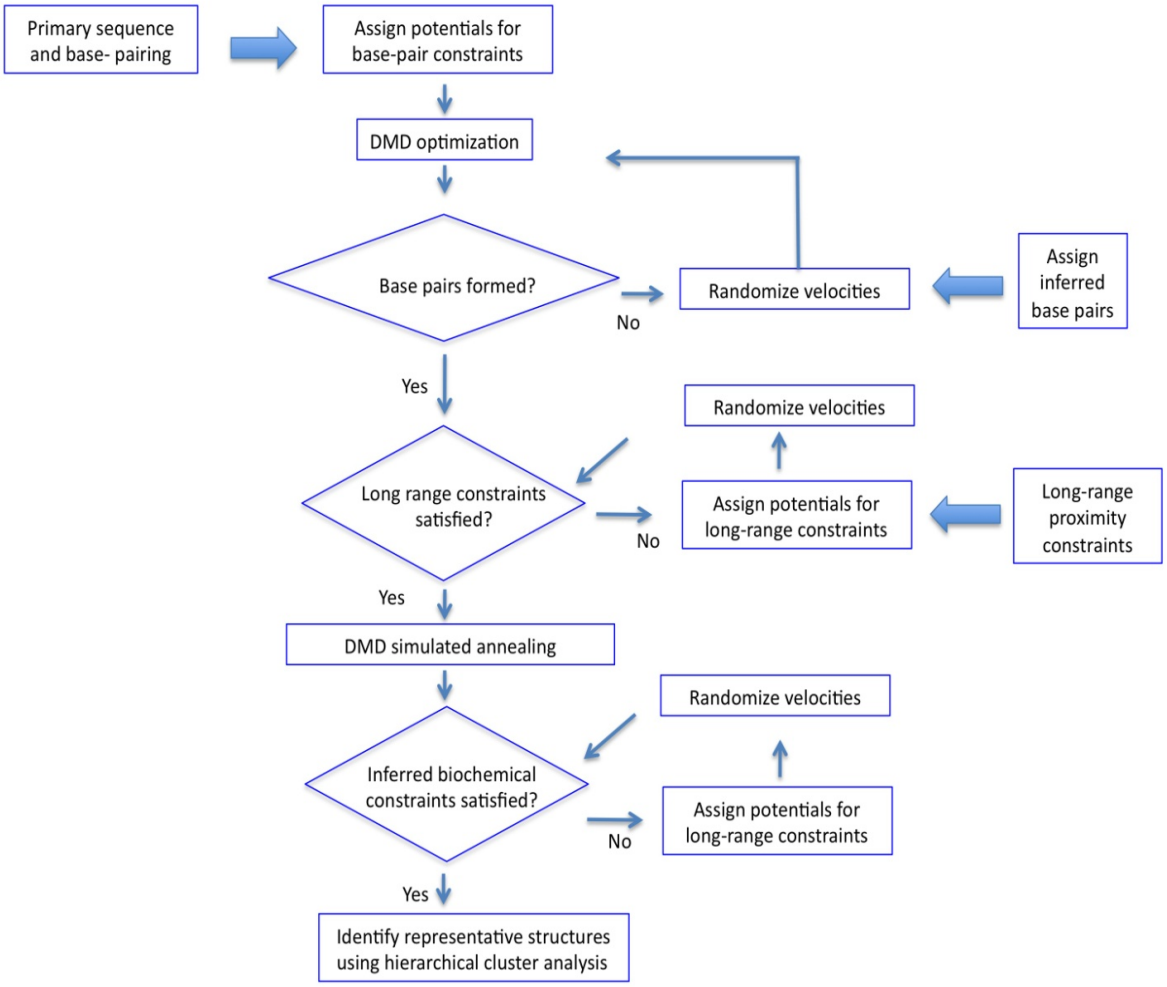

Figure S11. Algorithm for DMD refinement.

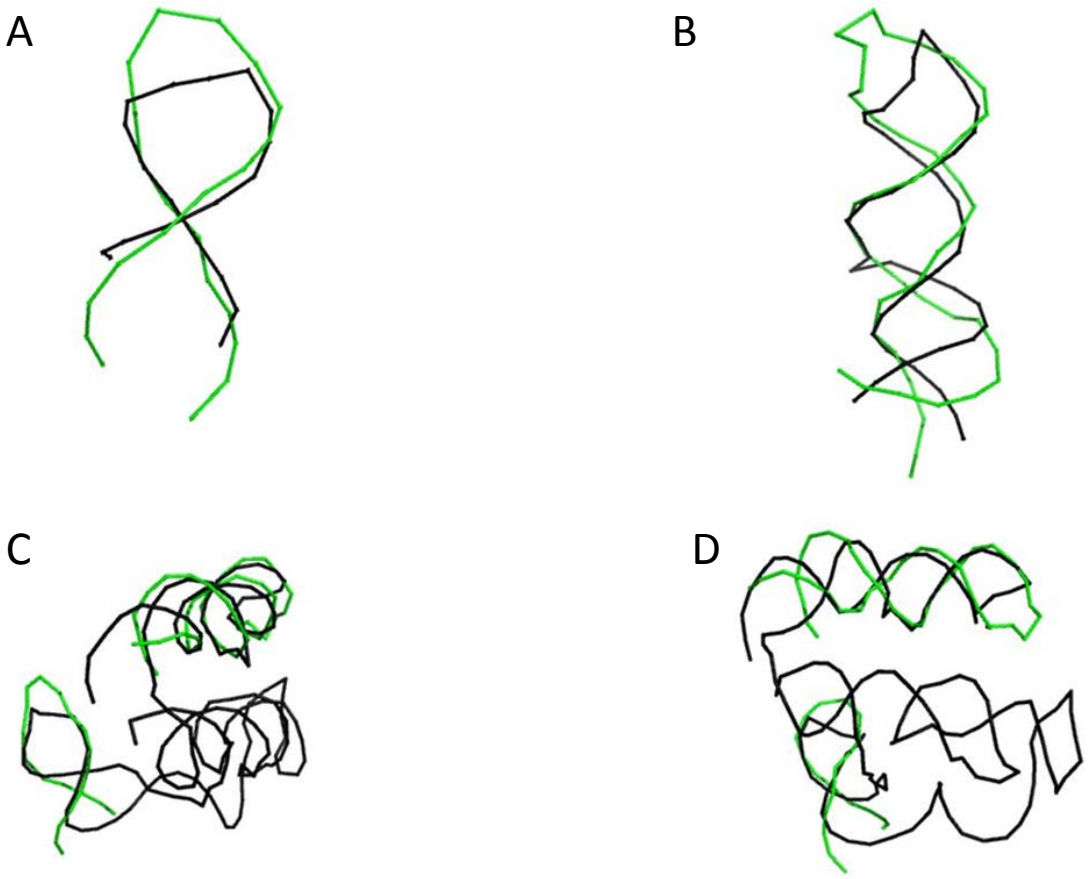

Figure S12. Alignment of structures from DMD simulations to NMR derived coordinates. (A) The phosphate backbone of nucleotides 19-37 were aligned to NMR derived atomic coordinates of a helix 2 model. The structures aligned to within 1.5 Å. (B) The phosphate backbone of nucleotides 112-154 were aligned to NMR derived atomic coordinates of a helix 4 model. The structures aligned to within 5.4 Å of a stem IV. (C) and (D) The NMR coordinates for helix 2 and helix 4 were superimposed on a representative full length tTER DMD structure. The DMD model is shown in black while the NMR derived coordinates are shown in green.

Table S1. Structural probing of in vitro transcribed tTER[a]

tTER position	NMIA[b]	RNase ONE[c]	DMS[d]	DEP[e]	RNase T1[f]	RNase T1[g]	RNase T1[h]	RNase V1[i]	RNase V1[j]	RNase V1[k]
A1	CBD	CBD	CBD	CBD	CBD	CBD	CBD	CBD	CBD	CBD
U2	CBD	CBD	CBD	CBD	CBD	CBD	CBD	CBD	CBD	CBD
A3	CBD	CBD	CBD	CBD	CBD	CBD	CBD	CBD	CBD	CBD
C4	CBD	CBD		CBD	CBD	CBD	CBD	CBD	CBD	CBD
C5	CBD	CBD		CBD	CBD	CBD	CBD	CBD	CBD	CBD
C6	CBD	CBD		CBD	CBD	CBD	CBD	CBD	CBD	CBD
G7	CBD	CBD		CBD	CBD	+	CBD	+++		CBD
C8	CBD	CBD		CBD	CBD		CBD		+	CBD
U9	CBD	CBD		CBD	CBD		CBD			CBD
U10	+	CBD		CBD	CBD		CBD			CBD
A11	++	CBD	+++		CBD		CBD			CBD
A12	++	CBD	+++		CBD		CBD			CBD
U13	+	CBD			CBD		CBD			CBD
U14	++	CBD			CBD		CBD			CBD
C15	CBD	CBD	+++		CBD		CBD			CBD
A16	+	CBD	+++		CBD		CBD			CBD
U17	+	CBD			CBD		CBD			CBD
U18	-	CBD			CBD		CBD			CBD
C19	-	CBD			CBD		CBD		+	CBD
A20	-	CBD			CBD		CBD		++	CBD
G21	-	CBD			CBD	+++	CBD	+++	+++	CBD
A22	-	CBD	+		CBD		CBD	+	++	CBD
U23	-	CBD			CBD		CBD	+		CBD
C24	-	CBD			CBD		CBD	+	+	CBD
U25	-	CBD			CBD		CBD		+	CBD
G26	+	CBD			CBD	++	CBD			CBD
U27	+++	CBD					CBD			CBD
A28	+++	CBD	+++	+++			CBD			CBD
A29	++	CBD	++	+			CBD			CBD
U30	+++	CBD								
A31	+	CBD								
G32	-				+++	++			+	
A33	-									
A34	-		+						+	
C35	-							+		
U36	-									
G37	-					++				
U38	++	+++								
C39	++	+++	+++							++
A40	+++	+++	+							
U41	+++	+++								
U42	+++	+++								
C43	++	+++	+++							++
A44	+++		+++	+						
A45	+		+	+						
C46	-									
C47	-									
C48	-							+		
C49	-	+	++							++

tTER position	NMIA[b]	RNase ONE[c]	DMS[d]	DEP[e]	RNase T1[f]	RNase T1[g]	RNase T1[h]	RNase V1[i]	RNase V1[j]	RNase V1[k]
A50	+++	+	+++					+		++
A51	+	+	+++	+						+
A52	+++	+	+++	+						
A53	+	+		+					+	
A54	-	+							+	
U55	-	+							+	
C56	-	+							++	
U57	+	+							++	++
A58	+	+							+	++
G59	+	+			+	+++				
U60	+	+								
G61	-	+			+++	+++				
C62	+	+	+++					+		
U63	-	++						+	++	
G64	-	++			+++	+++		+	++	
A65	++	++								++
U66	++	++								
A67	+++	++	+	+					+	++
U68	+++	++							+	
A69	+++	++	+++	+++					++	
A70	+++	++	+++	+++					++	
C71	-		+++						++	
C72	++		+++		+				++	
U73	+				+				++	
U74	+	+							+	
C75	+	+								
A76	+									
C77	-								++	
C78	+	+							++	
A79	+++	+	+	+++					++	
A80	+++	+	+++	+						
U81	+++	+								
U82	+	+								
A83	-								++	
G84	-				+	+		+		
G85	-				+	+		+	+	
U86	-							+		
U87	+									++
C88	+	+++	+++							
A89	++	+++	+++	+++						
A90	++	+++	+++	+++						
A91	++	+++	++	+++						
U92	++	+++								
A93	++		+++	+++						
A94	++		+	+++						
G95	+				+	+++			+	+
U96	+++									+
G97	-				+	+++				
G98	-				+	+++				+
U99	+	+								
A100	++	+	+	+						
A101	++	+	+++	+						
U102	++									
G103	-								+++	

tTER position	NMIA[b]	RNase ONE[c]	DMS[d]	DEP[e]	RNase T1[f]	RNase T1[g]	RNase T1[h]	RNase V1[i]	RNase V1[j]	RNase V1[k]
C104	-							+	+++	
G105	-							+	+++	
G106	-				+				+++	
G107	-				+++				+++	+
A108	++	+++	+++							
C109	CBD	+++	+++							
A110	+++	+++	+++	+					+	
A111	+++		+++	+						
A112	++		++							
A113	+								+	
G114	-					+			+++	
A115	-									+
C116	-									
U117	+++	++								
A118	++		+							+
U119	+							+		
C120	-		+++							
G121	+++				+++	++			+++	
A122	+++	++	+++	+++						
C123	-									+
A124	+									+
U125	++									
U126	++									
U127	++							+++	+	
G128	-							+++	+	
A129	-					CBD	CBD	+++	CBD	CBD
U130	-					CBD	CBD	+	CBD	CBD
A131	+++					CBD	CBD		CBD	CBD
C132	-		CBD			CBD	CBD		CBD	CBD
A133	+++	+++	CBD	+++		CBD	CBD		CBD	CBD
C134	++	+++	CBD			CBD	CBD		CBD	CBD
U135	+++	+++	CBD			CBD	CBD		CBD	CBD
A136	+++	+++	CBD	+++		CBD	CBD		CBD	CBD
U137	+++	+++	CBD			CBD	CBD		CBD	CBD
U138	+++	+++	CBD			CBD	CBD		CBD	CBD
U139	+	+	CBD			CBD	CBD		CBD	CBD
A140	-	CBD	CBD			CBD	CBD		CBD	CBD
U141	-	CBD	CBD			CBD	CBD		CBD	CBD
C142	-	CBD	CBD			CBD	CBD		CBD	CBD
A143	-	CBD	CBD			CBD	CBD		CBD	CBD
A144	+	CBD	CBD			CBD	CBD		CBD	CBD
U145	+	CBD	CBD			CBD	CBD		CBD	CBD
G146	++	CBD	CBD		+	CBD	CBD		CBD	CBD
G147	+	CBD	CBD		+	CBD	CBD		CBD	CBD
A148	+	CBD	CBD			CBD	CBD		CBD	CBD
U149	+	CBD	CBD			CBD	CBD		CBD	CBD
G150	-	CBD	CBD		+	CBD	CBD		CBD	CBD
U151	-	CBD	CBD			CBD	CBD	+	CBD	CBD
C152	-	CBD	CBD			CBD	CBD	+++	CBD	CBD
U153	+	CBD	CBD			CBD	CBD	+	CBD	CBD
U154	+++	CBD	CBD			CBD	CBD	+++	CBD	CBD
A155	+++	CBD	CBD			CBD	CBD		CBD	CBD
U156	+++	CBD	CBD			CBD	CBD		CBD	CBD
U157	+++	CBD	CBD			CBD	CBD		CBD	CBD

tTER position	NMIA[b]	RNase ONE[c]	DMS[d]	DEP[e]	RNase T1[f]	RNase T1[g]	RNase T1[h]	RNase V1[i]	RNase V1[j]	RNase V1[k]
U158	+++	CBD	CBD			CBD	CBD		CBD	CBD
U159	+++	CBD	CBD			CBD	CBD		CBD	CBD

[a] Reported tTER footprinting results are listed. For each nucleotide, the reactivity with a specific reagent is given as CBD (result could be determined), - (unreactive to NMIA), + (low reactivity), ++ (moderate reactivity), +++ (high reactivity). The absence of a symbol was used for cases where no data were availability either from a lack of reactivity or the inability of the reagent to report on the position.

[b] SHAPE reactivity using NMIA of tTER.

[c] RNaseONE digestion of tTER [12].

[d] Dimethyl sulfate footprint of tTER [13].

[e] Diethylpyrocarbonate footprint of tTER [14].

[f] RNaseT1 digestion of tTER [14].

[g] RNase T1 digestion of tTER in rabbit reticulocyte lysate [15].

[h] RNase T1 digestion of tTER [12].

[i] RNase V1 digestion of tTER [14].

[j] RNase V1 digestion of tTER in rabbit reticulocyte lysate [15].

[k] RNase V1 digestion of tTER [12].

Table S2. Structural probing of tTER bound to tTERT or the tTERT RNA binding domain[a]

tTER Nucleotide	NMIA[b]	RNase ONE[c]	DMS[d]	RNase T1[e]	RNase T1[f]	RNase V1[g]	RNase V1[h]
A1	CBD	CBD	CBD	CBD	CBD	CBD	CBD
U2	CBD	CBD	CBD	CBD	CBD	CBD	CBD
A3	CBD	CBD	CBD	CBD	CBD	CBD	CBD
C4	CBD	CBD		CBD	CBD	CBD	CBD
C5	CBD	CBD		CBD	CBD	CBD	CBD
C6	CBD	CBD		CBD	CBD	CBD	CBD
G7	CBD	CBD			CBD		CBD
C8	CBD	CBD		+	CBD		CBD
U9	CBD	CBD			CBD		CBD
U10	++	CBD			CBD		CBD
A11	++	CBD	+		CBD		CBD
A12	++	CBD	+		CBD		CBD
U13	++	CBD			CBD		CBD
U14	++	CBD			CBD		CBD
C15	-	CBD			CBD		CBD
A16	-	CBD			CBD		CBD
U17	-	CBD			CBD		CBD
U18	-	CBD			CBD		CBD
C19	-	CBD			CBD	+	CBD
A20	-	CBD			CBD	++	CBD
G21	-	CBD		+	CBD	+++	CBD
A22	-	CBD	+		CBD	++	CBD
U23	-	CBD			CBD	++	CBD
C24	-	CBD			CBD	++	CBD
U25	-	CBD			CBD	++	CBD
G26	-	CBD		++	CBD		CBD
U27	++	CBD			CBD		CBD
A28	+++	CBD	+		CBD		CBD
A29	+	CBD			CBD		CBD
U30	+++	CBD					
A31	-	CBD					
G32	-			+	+		
A33	-						
A34	-						+
C35	-					+	+
U36	-						+
G37	-			+	+	+	
U38	-	++					
C39	+	++					++
A40	+++	++	+				
U41	+++	++					
U42	+++	++					+++
C43	CBD	++	+++				++
A44	++		+++				
A45	+		+++				
C46	-		+++				+
C47	-		+++				++
C48	-		+++			+	++
C49	-	++	+++			++	++
A50	+++	++	+++			++	++

tTER Nucleotide	NMIA[b]	RNase ONE[c]	DMS[d]	RNase T1[e]	RNase T1[f]	RNase V1[g]	RNase V1[h]
A51	+	++	+++			++	+
A52	++	++	+++			+	
A53	++	++	+++				
A54	++	++	+				
U55	++	++				+	++
C56	+	++	+			++	++
U57	++	++				++	++
A58	+++	++	+			+	+
G59	+++	++		+++	+		+
U60	+++	++					+
G61	++	++		+++	+		++
C62	+	++					++
U63	++	++				++	++
G64	++	++		+++	+	++	
A65	+++	++	+				+
U66	CBD	++	++				
A67	+++	++	++			+	+
U68	+++	++				+	
A69	++	++				++	
A70	+	++				++	
C71	-					++	
C72	-					++	
U73	-					++	
U74	+	+				+	
C75	+	+					
A76	+					+	
C77	-					+	
C78	-	+				+	
A79	++	+				+	
A80	++	+				+	
U81	++	+					+
U82	+	+					+
A83	-				+		+++
G84	-			+	+	++	
G85	-			+		+++	
U86	+						++
U87	++						
C88	CBD	+++					
A89	++	+++					
A90	+	+++					
A91	++	+++					
U92	++	+++					
A93	++						
A94	++						
G95	+			+	+	+	+
U96	++						+
G97	-			+	+		
G98	-			+	+		+
U99	+	+					
A100	+++	+	++				
A101	CBD	+	+				
U102	+++						
G103	-						++
C104	-					+++	++

tTER Nucleotide	NMIA[b]	RNase ONE[c]	DMS[d]	RNase T1[e]	RNase T1[f]	RNase V1[g]	RNase V1[h]
G105	-					+++	+
G106	-					++	
G107	-						+
A108	CBD		++				
C109	CBD	+++	++				
A110	+++	+++	++			+	
A111	+++		++				
A112	+		+				
A113	-					+	
G114	-			+	+	+	
A115	-					+	+
C116	-					+	
U117	++	++				+	
A118	-					+	+
U119	CBD					+	
C120	-					+	
G121	+++			++	+		
A122	+++	++					
C123	-						+
A124	+						+
U125	CBD						
U126	+						
U127	++					+	
G128	CBD					+	
A129	-			CBD		CBD	
U130	-			CBD		CBD	
A131	+			CBD		CBD	
C132	-	++	CBD	CBD		CBD	
A133	++	++	CBD	CBD		CBD	
C134	+	++	CBD	CBD		CBD	
U135	++	++	CBD	CBD		CBD	
A136	+++		CBD	CBD		CBD	
U137	+++		CBD	CBD		CBD	
U138	+++		CBD	CBD		CBD	
U139	-		CBD	CBD		CBD	
A140	-	CBD	CBD	CBD		CBD	
U141	-	CBD	CBD	CBD		CBD	
C142	-	CBD	CBD	CBD		CBD	
A143	-	CBD	CBD	CBD		CBD	
A144	-	CBD	CBD	CBD		CBD	
U145	CBD	CBD	CBD	CBD		CBD	
G146	CBD	CBD	CBD	CBD		CBD	
G147	-	CBD	CBD	CBD	CBD	CBD	CBD
A148	-	CBD	CBD	CBD	CBD	CBD	CBD
U149	-	CBD	CBD	CBD	CBD	CBD	CBD
G150	CBD	CBD	CBD	CBD	CBD	CBD	CBD
U151	CBD	CBD	CBD	CBD	CBD	CBD	CBD
C152	-	CBD	CBD	CBD	CBD	CBD	CBD
U153	+	CBD	CBD	CBD	CBD	CBD	CBD
U154	CBD	CBD	CBD	CBD	CBD	CBD	CBD
A155	+++	CBD	CBD	CBD	CBD	CBD	CBD
U156	+++	CBD	CBD	CBD	CBD	CBD	CBD
U157	+++	CBD	CBD	CBD	CBD	CBD	CBD
U158	+++	CBD	CBD	CBD	CBD	CBD	CBD

tTER Nucleotide	NMIA[b]	RNase ONE[c]	DMS[d]	RNase T1[e]	RNase T1[f]	RNase V1[g]	RNase V1[h]
U159	+++	CBD	CBD	CBD	CBD	CBD	CBD

[a] Reported tTER footprinting results are listed. For each nucleotide, the reactivity with a specific reagent is given as CBD (result could be determined), - (unreactive to NMIA), + (low reactivity), ++ (moderate reactivity), +++ (high reactivity). The absence of a symbol was used for cases where no data were availability either from a lack of reactivity or the inability of the reagent to report on the position.
[b] SHAPE reactivity using NMIA of tTER in the soluble, affinity purified, minimal telomerase complex using full-length tTERT.
[c] RNaseONE digestion of tTER bound to tTERT(1-516).
[d] In cell dimethyl sulfate foortprinting of tTER [13].
[e] Ribonuclease T1 digestion of tTER bound to tTERT in crude rabbit reticulocyte lysates. [15].
[f] Ribonuclease T1 digestion of tTER bound to tTERT(1-516) [12].
[g] Ribonuclease V1 digestion of tTER bound to tTERT in crude rabbit reticulocyte lysates. [15].
[h] Ribonuclease V1 digestion of tTER bound to tTERT(1-516) [12].

References for supporting material.

(1) Deigan, K. E.; Li, T. W.; Mathews, D. H.; Weeks, K. M. *Proc. Natl. Acad. Sci.* **2009**, *106*, 97.
(2) McGinnis, J. L.; Duncan, C. D. S.; Weeks, K. M.; Daniel, H. *Methods Enzymol.* **2009**, *468*, 67.
(3) Wilkinson, K. A.; Gorelick, R. J.; Vasa, S. M.; Guex, N.; Rein, A.; Mathews, D. H.; Giddings, M. C.; Weeks, K. M. *PLoS Biol.* **2008**, *6*, e96.
(4) Duncan, C. D.; Weeks, K. M. *Biochemistry* **2008**, *47*, 8504.
(5) Reuter, J. S.; Mathews, D. H. *BMC Bioinformatics* **2010**, *11*, 129.
(6) Mathews, D. H. *RNA* **2004**, *10*, 1178.
(7) McCaskill, J. S. *Biopolymers* **1990**, *29*, 1105.
(8) Mathews, D. H.; Disney, M. D.; Childs, J. L.; Schroeder, S. J.; Zuker, M.; Turner, D. H. *Proc. Natl. Acad. Sci.* **2004**, *101*, 7287.
(9) Lu, Z. J.; Gloor, J. W.; Mathews, D. H. *RNA* **2009**, *15*, 1805.
(10) Bellaousov, S.; Mathews, D. H. *RNA* **2010**, *16*, 1870.
(11) Mathews, D. H.; Sabina, J.; Zuker, M.; Turner, D. H. *J. Mol. Biol.* **1999**, *288*, 911.
(12) Berman, A. J.; Gooding, A. R.; Cech, T. R. *Mol. Cell. Biol.* **2010**, *30*, 4965.
(13) Zaug, A. J.; Cech, T. R. *RNA* **1995**, *1*, 363.
(14) Bhattacharyya, A.; Blackburn, E. H. *EMBO J.* **1994**, *13*, 5721.
(15) Sperger, J. M.; Cech, T. R. *Biochemistry* **2001**, *40*, 7005.